ResearchGate

See discussions, stats, and author profiles for this publication at: https://www.researchgate.net/publication/5846123

Probing the MgATP-Bound Conformation of the Nitrogenase Fe Protein by Solution Small-Angle X-ray Scattering †

ARTICLE *in* BIOCHEMISTRY · JANUARY 2008

Impact Factor: 3.02 · DOI: 10.1021/bi700446s · Source: PubMed

CITATIONS
8

READS
20

7 AUTHORS, INCLUDING:

Ranjana Sarma
Karolinska Institutet
7 PUBLICATIONS **198** CITATIONS

SEE PROFILE

David Mulder
National Renewable Energy Laboratory
22 PUBLICATIONS **450** CITATIONS

SEE PROFILE

Robert K Szilagyi
University of Pannonia, Veszprém
91 PUBLICATIONS **2,683** CITATIONS

SEE PROFILE

Lance Seefeldt
Utah State University
136 PUBLICATIONS **5,388** CITATIONS

SEE PROFILE

Available from: Ranjana Sarma
Retrieved on: 30 January 2016

Probing the MgATP-Bound Conformation of the Nitrogenase Fe Protein by Solution Small-Angle X-ray Scattering†

Ranjana Sarma,‡ David W. Mulder,‡ Eric Brecht,‡ Robert K. Szilagyi,‡ Lance C. Seefeldt,§ Hiro Tsuruta,‖ and John W. Peters*,‡

Department of Chemistry and Biochemistry, Montana State University, Bozeman, Montana 59717, Stanford Synchrotron Radiation Laboratory, Stanford Linear Accelerator Center, Stanford University, MS 69, 2575 Sand Hill Road, Menlo Park, California 94025, and Department of Chemistry and Biochemistry, Utah State University, Logan, Utah 84322

Received March 6, 2007; Revised Manuscript Received September 30, 2007

ABSTRACT: The MgATP-bound conformation of the Fe protein of nitrogenase from *Azotobacter vinelandii* has been examined in solution by small-angle X-ray scattering (SAXS) and compared to existing crystallographically characterized Fe protein conformations. The results of the analysis of the crystal structure of an Fe protein variant with a Switch II single-amino acid deletion recently suggested that the MgATP-bound state of the Fe protein may exist in a conformation that involves a large-scale reorientation of the dimer subunits, resulting in an overall elongated structure relative to the more compact structure of the MgADP-bound state. It was hypothesized that the Fe protein variant may be a conformational mimic of the MgATP-bound state of the native Fe protein largely on the basis of the observation that the spectroscopic properties of the [4Fe-4S] cluster of the variant mimicked in part the spectroscopic signatures of the native nitrogenase Fe protein in the MgATP-bound state. In this work, SAXS studies reveal that the large-scale conformational differences between the native Fe protein and the variant observed by X-ray crystallography are also observed in solution. In addition, comparison of the SAXS curves of the Fe protein nucleotide-bound states to the nucleotide-free states indicates that the conformation of the MgATP-bound state in solution does not resemble the structure of the variant as initially proposed, but rather, at the resolution of this experiment, it resembles the structure of the nucleotide-free state. These results provide insights into the Fe protein conformations that define the role of MgATP in nitrogenase catalysis.

Biological nitrogen fixation is a critical step in the global nitrogen cycle that is carried out exclusively by prokaryotes. The reduction of N_2 to two NH_3 molecules is catalyzed by the enzyme nitrogenase that exists in Mo-, V-, and Fe-only forms. Mo nitrogenase is the most extensively studied form and consists of two oxygen sensitive protein components termed the Fe protein and the MoFe protein (*1*). The Fe protein is a homodimer (∼64 kDa) with a single [4Fe-4S] cluster bridging the two subunits with each subunit possessing a single site for MgATP binding and hydrolysis. The MoFe protein, an $\alpha_2\beta_2$ heterotetramer (∼230 kDa), has two types of complex iron−sulfur clusters termed the P-clusters (8Fe-7S) and the FeMo cofactors (Mo-7Fe-9S-homocitrate), the latter serving as the sites for N_2 binding and reduction (*2*−*4*).

During catalysis, the Fe protein and the MoFe protein associate with the transfer of a single electron from the Fe protein to the MoFe protein coupled to the hydrolysis of two MgATP molecules, one of each subunit of the Fe protein. Since eight electrons must be transferred to the MoFe protein for the reduction of one N_2 molecule to two NH_3 molecules and the reduction of two protons yielding H_2, multiple cycles of component protein interaction are required for the complete nitrogenase catalytic cycle. One of the more intriguing aspects of the nitrogenase mechanism is the involvement of MgATP.[1] The coupling of MgATP hydrolysis to multiple-electron reduction reactions is unusual in biology. More common is the coupling of nucleoside triphosphate hydrolysis to a cellular process such as metabolic regulation (*5*−*7*), protein synthesis (*8*, *9*), DNA repair (*10*, *11*), or muscle contraction (*12*−*14*). Details of the role of MgATP binding and hydrolysis in nitrogenase catalysis remain unknown, although it is assumed to function to gate the unidirectional flow of electrons from the Fe protein toward

† This work was supported by National Institutes of Health Grants GM069938 (J.W.P.) and GM59087 (L.C.S.). Portions of this research were carried out at the Stanford Synchrotron Radiation Laboratory, a national user facility operated by Stanford University on behalf of the U.S. Department of Energy, Office of Basic Energy Sciences. The SSRL Structural Molecular Biology Program is supported by the Department of Energy, Office of Biological and Environmental Research, and by the National Institutes of Health, National Center for Research Resources, Biomedical Technology Program, and the National Institute of General Medical Sciences.

* To whom correspondence should be addressed. Phone: (406) 994-7211. Fax: (406) 994-7212. E-mail: john.peters@chemistry.montana.edu.

‡ Montana State University.

§ Utah State University.

‖ Stanford University.

[1] Abbreviations: MgADP, magnesium adenosine 5′-diphosphate; MgATP, magnesium adenosine 5′-triphosphate; SAXS, small-angle X-ray scattering; R_g, radius of gyration; $P(r)$, electron pair distribution function; D_{max}, maximum diameter; NSD, normalized spatial discrepancy.

10.1021/bi700446s CCC: $37.00 © 2007 American Chemical Society
Published on Web 11/15/2007

the substrate (*1*). The ability to accumulate multiple electrons on the MoFe protein is necessary to complete the catalytic cycle since N_2 does not bind at the FeMo cofactor until the enzyme is reduced by several electrons (*2*, *15*−*17*).

The binding of nucleotides to the Fe protein is known to induce protein conformational changes as evidenced by changes in the spectroscopic properties of the [4Fe-4S] cluster (*18*−*27*). While these spectroscopic methods reflect changes in the electronic properties of the [4Fe-4S] cluster, they do not directly access changes to the overall structure of the Fe protein. To gain insights into nucleotide-dependent protein conformational states of the Fe protein, a number of X-ray crystal structures of Fe protein and Fe protein−MoFe protein complexes without and with bound nucleotides have been determined (*28*−*35*). These structures provide insights into the interactions of nucleotides with Fe protein, the role of the signal transduction pathways and switch regions, and intermolecular electron transfer between Fe and MoFe proteins. These studies have clearly shown that the Fe protein is capable of undergoing conformational changes manifested mainly as the rigid body reorientation of the two subunits. On the basis of these studies, models for the conformational changes and the interaction that occur within the nitrogenase complex have been proposed. The crystal structure of a key state in defining Fe protein nucleotide-dependent conformational change, the MgATP-bound state, has not been elucidated.

Although the structure of a true MgATP-bound state of the Fe protein has not been determined, we have recently characterized the X-ray crystal structure of a variant of the Fe protein with a single deletion in the switch region that connects the nucleotide binding site to the [4Fe-4S] cluster (*33*, *34*). The crystal structure of the L127Δ Fe protein shows a structure strikingly different from the previously determined structures, characterized by a large rigid-body reorientation of the two subunits. Spectroscopic and biochemical studies of this variant protein have revealed similarities in the spectroscopic properties of the nucleotide-free form of the L127Δ Fe protein and the MgATP-bound state of the Fe protein (*36*). The L127Δ Fe protein is not capable of nitrogen reduction, but it can form a stable complex with the MoFe protein in the absence of nucleotides that resembles the native Fe protein−MoFe protein complex stabilized by MgADP-tetrafluoroaluminate (*37*, *38*). Although the characterization of the [4Fe-4S] cluster of this variant provides support for the idea that the L127Δ Fe protein somehow mimics several aspects of the MgATP-bound native Fe protein (*36*), the relationship between the variant and the MgATP-bound state from the perspective of protein structure has not yet been examined.

Recent structural work in which a number of nitrogenase complexes were stabilized in the presence of nucleotides and nucleotide analogues favors a different model in which Fe protein conformational changes were much less pronounced (*32*). From the results of this work, it was proposed that the cycle of complex association, coupled nucleotide hydrolysis and electron transfer, and complex dissociation involved the binding of the different states of the Fe protein to the MoFe protein at different sites. In the work presented here, small-angle solution X-ray scattering studies have been implemented to analyze the structure of the Fe protein in nucleotide-bound conformations to critically evaluate our hypotheses with respect to nucleotide-dependent conformational states and to determine the relationship between the structure of the authentic MgATP-bound form and the previously crystallographically characterized conformations.

EXPERIMENTAL PROCEDURES

Protein Purification. Both the native Fe protein and the L127Δ Fe protein of nitrogenase from *Azotobacter vinelandii* were purified as described previously (*18*). The proteins were buffer-exchanged into 20% glycerol buffer at pH 7.5 with 0.5 M NaCl by Sephacryl-200 gel filtration chromatography. The native Fe protein was concentrated to 33 mg/mL, and the L127Δ Fe protein was concentrated to 100 mg/mL using an Amicon concentration apparatus under argon pressure and stored in liquid nitrogen.

Sample Preparation. All samples for the SAXS experiments were prepared in a glovebox (Vacuum Atmospheres, Hawthome, MA) operating under a N_2 atmosphere at less than 1 ppm of oxygen. All buffers, which contained 20% glycerol and 5 mM dithionite, were degassed under vacuum in sealed Wheaton vials in an atmosphere of 100% N_2. To ensure the integrity of MgADP- and MgATP-bound samples, nucleotide stock solutions (100 mM) were prepared no more than 15 min prior to data collection. To ensure nucleotide saturation, three different nucleotide concentrations were initially used, specifically 1 mM ATP/ADP with 2 mM $MgCl_2$, 5 mM ATP/ADP with 10 mM $MgCl_2$, and 10 mM ATP/ADP with 20 mM $MgCl_2$. There were no discernible differences observed at the different concentrations, and a final nucleotide concentration of 5 mM (a 20−25-fold molar excess) was used throughout the experiment to ensure saturation.

Data Collection. SAXS data were collected at beamline 4-2 (*39*) at the Stanford Synchrotron Radiation Laboratory (SSRL) on five different occasions. On the first two occasions, conventional flat-window cells with thin mica windows were used. For data collections in which all of the data presented herein were recorded, a continuous flow cell incorporating a thin wall X-ray capillary was used. The flow cell was attached to a computer-controlled syringe dispenser (Hamilton 500 series, 250 μL syringe) via oxygen-impermeable tubing, and the samples were injected into the flow cell system from sealed vials under mildly positive N_2 pressure to maintain anaerobic conditions. The sample volume for each run was 80 μL, and the dispenser was set in a continuous loop to allow the sample to pass 30 μL in the forward and reverse direction (4 μL/s) relative to the X-ray beam position. The continuous flow of the sample evenly distributed 20 X-ray exposures, each lasting 10 s, over the majority of the sample aliquot. This data collection strategy proved to be highly effective, and the effects of X-ray radiation damage and protein aggregation, which initially had been observed, were eliminated. To maintain anaerobic conditions throughout the experiments, we flushed the flow cell with anoxic buffer after each run. The capillary cell was maintained at 20 °C throughout the measurements. The detector pixels were calibrated to the momentum transfer Q, which equals $4\pi \sin(\theta)/\lambda$ (θ is one-half of the scattering angle and λ is the wavelength) using the (100) and related higher-order reflections from a cholesterol myristate or silver behanate powder sample. Fe protein data were collected at

an incident beam energy of 8700 eV, 8950 eV, or 11 keV using a MARCCD165 detector (MarUSA, Evanston, IL) 1 m from the sample cell.

Calibration. Lysozyme was used as a calibration standard for experimental setup and measured intensities as described previously (*40*). Reagent-grade lysozyme (Fischer Scientific) was used to make up solutions [10 mM ammonium acetate (pH 5.0) and 150 mM NaCl] at four different concentrations: 2.5, 5, 10, and 20 mg/mL. Each of the samples was run in triplicate at 8950 eV. The experimental scattering curves were compared to the theoretical scattering curve generated using Protein Data Bank crystal structure 193L (*41*) in CRYSOL (*42*).

Potential for artifacts arising from Fe fluorescence or anomalous scattering effects from the [4Fe-4S] cluster in the Fe protein was probed by measuring scattering curves of buffer solutions containing different concentrations of Fe standards. Scattering curves were collected for ferrous ammonium sulfate at 0.1, 0.3, and 0.7 mM in buffer solution at three different energies: 7050 eV, 7150 eV (near the Fe edge), and 8950 eV (remote relative to the Fe edge). A Vortex silicon drift detector (SII NanoTechnology USA, Northridge, CA) was also used to evaluate the potential contribution of Fe fluorescence in the scattering data.

Data Analysis. The two-dimensional images from the detector were azimuthally integrated, scaled for beam intensities, frame-averaged, and background-subtracted with *MarParse* (*39*) to yield the scattering curves. Each experimental run was carried out at least in duplicate to ensure reproducibility. In addition, scattering curves of each corresponding buffer and nucleotide solution were subtracted from the individual protein scattering curves to eliminate any scattering contributions of the buffer solution. The data statistics of a preceding buffer solution measurement established the amount of systematic error in the data collection system and propagated to the protein scattering data upon buffer curve subtraction in addition to the standard deviation from the protein measurement. Radii of gyration (R_g) values for native Fe protein samples (both nucleotide-free and nucleotide-bound states) were obtained from the Guinier plots using the first 20 intensity points beyond the beam stop in the Q range of 0.023−0.052 Å^{-1}. In the case of the L127Δ Fe protein samples, R_g values were estimated using a Q range of 0.022−0.045 Å. Theoretical curves were generated with CRYSOL (*42*) from the crystal structure of the nucleotide-free native Fe protein (2NIP) (*30*) and the crystal structure of the nucleotide-free L127Δ Fe protein (1RW4) (*33*). The electron pair distance distribution function, $P(r)$, was calculated using GNOM (*43*). In these calculations, scattering intensity points in the Q range of ∼0.02−0.3 Å^{-1} were used. The maximum distance (D_{max}) values of 70 and 80 Å were assumed for the native and L127Δ Fe protein calculations, respectively, on the basis of the dimensions obtained from the corresponding crystal structures. These D_{max} values were verified to be valid in solution by running GNOM with varying D_{max} values. The best results were obtained at D_{max} values of 70 Å (native) and 80 Å (L127Δ) for the nucleotide-free states and at D_{max} values of 75 Å (native) and 80 Å (L127Δ) for the nucleotide-bound states.

Ab initio shape reconstructions of the Fe protein in the nucleotide-free state and the L127Δ Fe protein were calculated with DAMMIN (*44*). In this particular work, all DAMMIN calculations were constrained to 2-fold symmetry and were run 10 times to check for reproducibility of model construction. The 10 separate, but similar, three-dimensional structure models obtained by DAMMIN for each condition were spatially aligned and also analyzed for spatial discrepancy by SUPCOMB (*45*) which was run as a subprocess of DAMAVER (*46*). In this analysis, dissimilar models are rejected and a most probable model representing the most populated volume among the 10 models is given.

RESULTS AND DISCUSSION

Several structures of the nitrogenase Fe protein have been determined, and their characterization has revealed that the protein can exist in several different conformations (*28*−*32*). The main differences among these conformations are manifested in different orientations of the individual subunits with respect to one another. This indicates that during catalysis the Fe protein undergoes conformational changes upon nucleotide binding, complex association, and dissociation, which tune the spectroscopic properties of the Fe protein's [4Fe-4S] cluster, modulate the distance between intermolecular redox partners (Fe protein [4Fe-4S] cluster and MoFe protein P cluster), and promote MgATP hydrolysis.

The overall differences in the dimensions of the Fe protein in different conformations from crystal structures, shown in Figure 1, indicate that the Fe protein can exist in molecular shapes that range from a more globular protein, as observed for the nucleotide-free native Fe protein (72 Å × 51 Å × 50 Å), to a more open or elongated shape, as observed for the L127Δ Fe protein (87 Å × 46 Å × 60 Å). The dramatic conformational difference observed between the crystal structures of native and L127Δ Fe protein was not anticipated. There are limited interactions between the subunits in the structure of the L127Δ Fe protein, suggesting a potentially higher degree of flexibility of the structure in comparison to the more globular compact conformations of the native nucleotide-free Fe protein. The limited interactions between the subunits of the L127Δ Fe protein coupled with the large differences observed between the native structure and the variant structure make it necessary to investigate whether the observed structure predominates in solution or whether the crystalline lattice itself is stabilizing a local energy minimum of an overall conformationally dynamic L127Δ Fe protein.

The structure of the L127Δ Fe protein was probed using SAXS to examine if the structure observed by crystallography was present as a predominant structure in solution. The scattering curves of globular compact proteins are noticeably different from the curves of the proteins having elongated or ellipsoid shapes. The extent of the differences between the conformation of the L127Δ Fe protein and the native Fe protein is large enough to result in discernible differences between the respective scattering curves. Theoretical scattering curves for the crystal structures and their R_g values for two conformations of the Fe protein are shown in Figure 1C. The structure of the more elongated L127Δ Fe protein has a larger anticipated radius of gyration because the elongated shape has a longer largest dimension. In addition to the larger R_g value, clear differences exist in the overall shape of the theoretical curves, especially in the Q

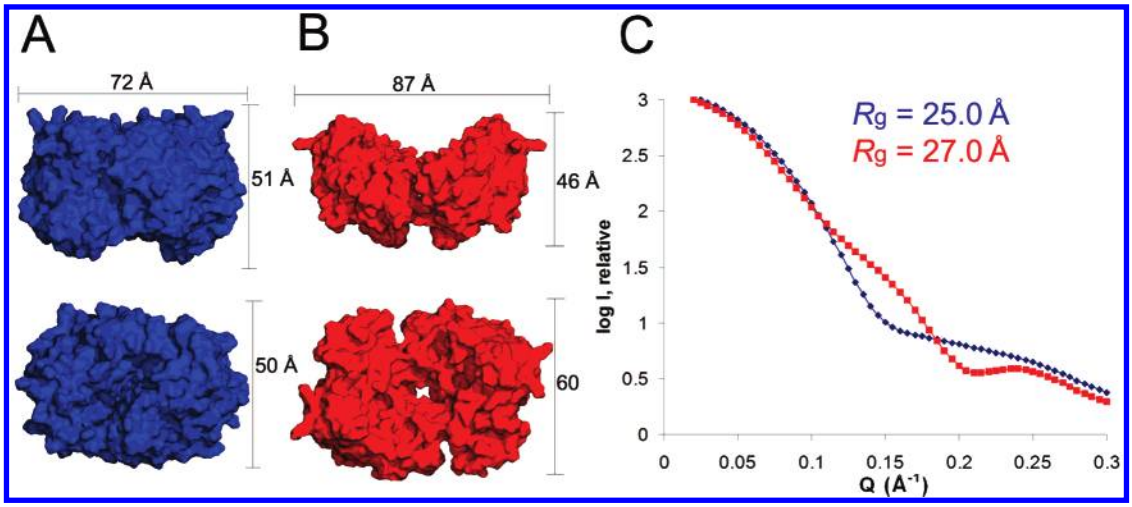

FIGURE 1: Surface renderings and maximum dimensions of the nitrogenase Fe protein in different structural conformations, including (A) the native nucleotide-free (2NIP) state (blue) and (B) the L127Δ nucleotide-free (1RW4) state (red). The two views of the Fe protein showing are separated by a 90° rotation about the horizontal axis. (C) Theoretical scattering curves obtained from CRYSOL for the crystal structures of Fe protein in the conformations shown in panels A and B with the same coloring scheme.

range of 0.1−0.2 $Å^{-1}$. The scattering data in this Q range are more sensitive to subtle conformational differences than R_g alone would indicate and can be exploited in distinguishing the Fe protein conformational states.

The first set of experimental runs, for both the native and L127Δ Fe proteins, were carried out at three different protein concentrations, 5, 10, and 20 mg/mL. A decrease in the R_g values as a function of concentration for both the native Fe protein (25.3 Å for 5 mg/mL, 22.7 Å for 10 mg/mL, and 21.3 Å for 20 mg/mL) and the L127Δ Fe protein (28.3 Å for 5 mg/mL and 25.6 Å for 20 mg/mL) were reproducibly observed, indicative of some repulsive interparticle interference. Subsequent measurements were conducted at a concentration of 5 mg/mL to limit interference since high-quality data with good signal could be obtained.

The experimental scattering curves of the solution structures of the nucleotide-free states of the native Fe protein and L127Δ Fe protein differences are shown in Figure 2A. The curves are consistent with the salient features of the theoretical curves for the two proteins based on the known structures of the proteins obtained by crystallography (Figure 1C), including the key distinguishing differences observed in the Q range of 0.1−0.2 $Å^{-1}$. Additionally, the R_g values obtained from the Guinier plots (Figure 2A inset) for the native Fe protein (25.3 ± 0.1 Å) and the L127Δ Fe protein (28.3 ± 0.1 Å) are near the simulated values of 25.0 and 27.0 Å, respectively (Figure 1C). The R_g value for the L127Δ is nearly ∼1 Å larger than the simulated curves, but clearly, the differences in comparing the native and L127Δ Fe protein are consistent with the observation that the native Fe protein exists in a more compact state and the L127 Fe protein is more elongated in structure. The lack of a precise fit to the simulated curve may, however, suggest that the crystalline lattice in the L127Δ Fe protein may be imposing some structural constraints on the conformation. To validate if the anticipated molecular shape of the native Fe protein and the L127Δ Fe protein is consistent with the observed scattering curves, the scattering data were analyzed by the indirect Fourier transform method using GNOM. This analysis evaluates the electron pair distance distribution function of a protein molecule in solution and also gives an estimate of the R_g values. The R_g values obtained by GNOM for the native Fe protein and L127Δ Fe protein were 25.2 and 27.6 Å, respectively (Figure 2B). These values are similar to the values obtained using the Guinier plots (Figure 2A inset). The larger R_g value for the L127Δ Fe protein in solution is consistent with a more elongated structure as observed by crystallography.

The scattering curves can be further exploited to yield molecular envelopes that can be compared directly to the existing crystal structures. The most probable low-resolution structural models of the native Fe protein and the L127Δ Fe protein computed from the experimental scattering data using DAMMIN are shown in panels C and D of Figure 2. The average normalized spatial discrepancy (NSD) values over all independent models were 0.55 (±0.03) for the native Fe protein and 0.63 (±0.01) for the L127Δ Fe protein. One model for the L127Δ Fe protein was excluded by DAMAVER due to a slightly higher NSD value. The range of NSD values in all cases indicates satisfactory similarity among 9 or 10 individually computed models from which the most probable models were computed by DAMAVER. As indicated in Figure 2, the shape reconstructions generated from the experimental curves are consistent with the overall globular state of the native Fe protein versus the more elongated shape for the L127Δ Fe protein observed by X-ray crystallography (Figure 1).

Although the salient differences of the scattering profiles in comparing the native Fe protein and L127Δ Fe protein can be rationalized in the context of the differences in the simulated scattering curves, a close comparison of the simulated and experimental scattering curves of both proteins (Figure 3) reveals significant differences at the higher scattering angles (>0.15 $Å^{-1}$). The differences in the experimental data are reproducible and could be the result of slight conformational variation or conformational dynamics in solution in comparison to the crystal structure. The potential for the discrepancy to be associated with artifacts resulting from the experimental setup was addressed using the protein lysozyme as a calibration standard. With the setup

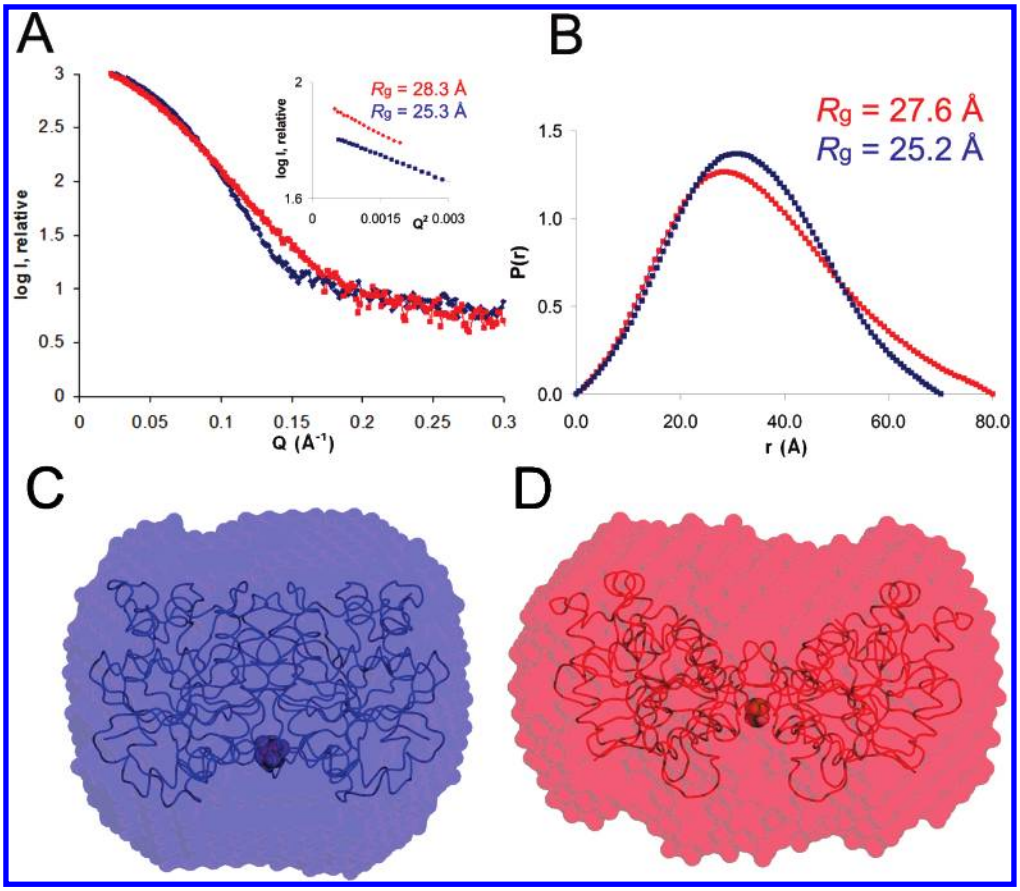

FIGURE 2: (A) Experimental scattering curves of the nucleotide-free native Fe protein (blue) and nucleotide-free L127Δ Fe protein (5 mg/mL) (red) and Guinier plots as the inset (A), where intensities are artificially offset to aid comparison. (B) Electron pair distribution function plots generated from the scattering curves in panel A with calculated R_g values for the nucleotide-free forms of the native Fe protein (blue) and the L127Δ Fe protein (red). *Ab initio* low-resolution structural reconstruction from the scattering curves obtained using DAMMIN and the cartoon representation of the crystal structure of the native Fe protein (blue) (C) or nucleotide-free L127Δ Fe protein (red) (D) fitted manually into the DAMMIN envelope.

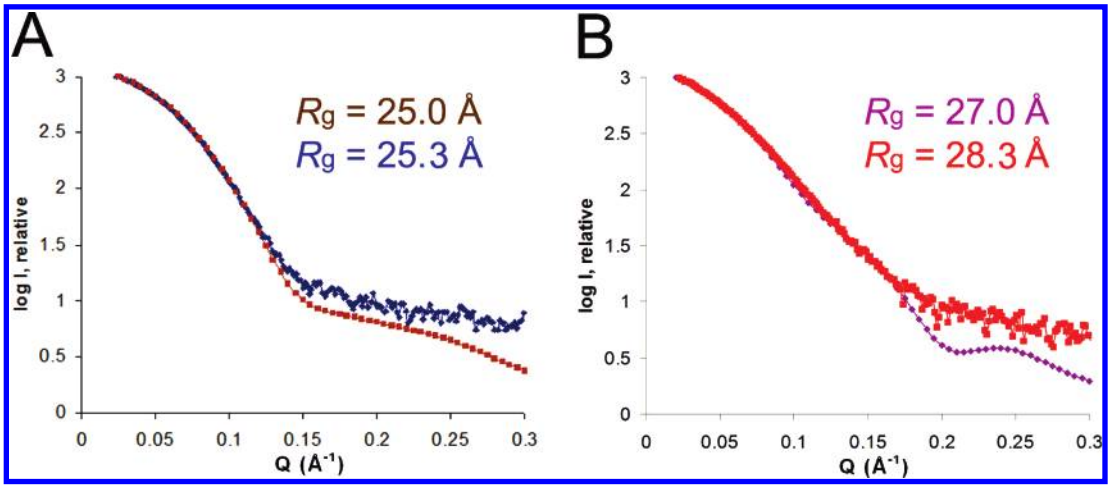

FIGURE 3: (A) Comparison of experimental scattering profiles of 5 mg/mL Fe protein (blue) and theoretical scattering curves of nucleotide-free native Fe protein (2NIP) (brown). (B) Comparison of experimental scattering profiles of 5 mg/mL L127Δ Fe protein (red) and theoretical scattering curves of nucleotide-free L127Δ Fe protein (1RW4) (violet).

used in this study, the experimental scattering data for lysozyme match exactly the simulated data computed from 193L using CRYSOL in the entire angular range, indicating that no artifacts were introduced at the level of the data collection or processing as the exactly the same procedures were employed as in the Fe protein runs. In addition, using lysozyme as a concentration standard for measured intensities as previously described (*40*) resulted in accurate estimation of the molecular mass of an Fe protein dimer in the range of 64 kDa.

Since the Fe protein contains a [4Fe-4S] cluster, the potential for artifacts occurring as a result of Fe fluorescence or anomalous scattering effects was also addressed by examining the scattering curves of Fe standards at different incidence X-ray beam energies. Scattering curves of ferrous ammonium sulfate solutions at 0.1, 0.3, and 0.7 mM at three

different incident energies (7050, 7150, and 8950 eV) near and remote relative to the Fe absorption edge (7113 eV) were examined to address the potential influence of the presence of Fe in the Fe protein on the experimental scattering data. These control experiments revealed a small contribution of Fe in the signal intensities of scattering curves and a small dependence on incident energies. However, the degree of the differences observed was orders of magnitude smaller than the intensity differences observed at the higher angles in our data, indicating that the X-ray fluorescence from the [4Fe-4S] cluster of the Fe protein is unlikely to be the source of the discrepancy between the Fe protein experimental and simulated scattering curves.

We have examined the possibility that the effect of higher solvent density could account for the differences between simulated and experimental scattering curves at higher angles. Modulating the values of solvent density in the calculation of the simulated scattering curves was found to significantly affect the intensity at higher angles. Increasing the values for the solvent density in the simulation to more correctly reflect the buffer density of experimental samples (20% glycerol and 0.5 M NaCl) resulted in better fits at the higher angles; for instance, a solvent electron density that is higher than that of pure water by 6% improved the χ^2 value from 8.6 to 5.3 for the native protein. Although there are likely to be small-scale differences in the solution and crystal structures of the Fe protein structures in the study, it can be concluded that the most significant differences at higher scattering angles are due to the higher solvent density in the experiments. Other subtle differences in the scattering curves may be a result of slight differences in the rigid body reorientation of the monomers in solution relative to the conformation observed in the crystal structures. We are currently attempting to optimize conditions to record accurate high-angle data to address this.

Having established that the difference between solution structures of the L127Δ Fe protein and the native Fe protein can be clearly distinguished using SAXS, we used this experimental method as a relative benchmark to ask the question of whether the different nucleotide-bound states resemble the conformations previously described. These studies are very important for the characterization of the MgATP-bound state since it has not yet been possible to obtain a structure of a MgATP-bound state of the native Fe protein crystallographically. For the MgADP-bound state of the native Fe protein, the structure has been crystallographically determined and the overall structure at a low resolution approximately resembles the conformation observed for the native Fe protein and in essence serves as an internal control for this analysis. Previous SAXS experiments probing the nucleotide-bound states of the Fe protein reported R_g values for the nucleotide-bound conformations very similar to those observed for the nucleotide-free native Fe protein (*47*, *48*). In the current study, the effects of binding of nucleotide to both the native and L127Δ Fe protein are examined in parallel to directly assess whether the L127Δ Fe protein is a mimic of the MgATP state as suggested previously (*33*).

The Fe protein was incubated with a molar excess of either MgATP or MgADP for 5−10 min prior to data collection. The significant molar excess of MgATP and the short time of incubation prior to data collection ensured that the Fe protein would be predominantly in the MgATP-bound form, with minimal hydrolysis to MgADP. The scattering curves for the native Fe protein (5 mg/mL) in the absence of nucleotides and in the presence of 5 mM MgADP or MgATP (>50-fold) are shown in Figure 4A. The scattering curves reveal that in the presence of either MgADP or MgATP, the structure of the Fe protein at the low resolution of the scattering experiment resembles the native state and does not undergo a large-scale conformational change to resemble the L127Δ Fe protein structure (Figure 2A). The estimations of the radius of gyration are very similar (∼25.0) to that obtained for the native Fe protein in the absence of nucleotide, and the key discriminating features of the scattering profile observed in the Q range of 0.1−0.2 $Å^{-1}$ resemble those of the native Fe protein more than those of the L127Δ Fe protein. This is consistent with the previously characterized crystallographic structure of the Fe protein with bound MgADP which was observed to exist in the same overall conformation as the nucleotide-free Fe protein. These results clearly indicate that the MgATP-bound state in solution does not exist in the elongated structure observed for the L127Δ Fe protein. Thus, in overall shape, the L127Δ Fe protein does not appear to faithfully mimic the conformation of the MgATP-bound state.

Although the addition of nucleotides does not result in the large-scale conformational change proposed in our previous work, comparison of the scattering curves of native and nucleotide-bound states indicates subtle differences (Figure 4A). Since the R_g and shape of the scattering curves are nearly the same, we can conclude the structures of the native and nucleotide bound states must be very similar. The small differences in the scattering curves of the native form in the presence (MgATP or MgADP) and absence of nucleotides could be a result of differences in the background subtraction. However, the relative differences in the native, MgADP, and MgATP scattering curves are also observed at higher (20 mg/mL) protein concentrations, and MgADP and MgATP should contribute very similarly to the background. Alternatively, the subtle differences could suggest that the states behave differently in solution which may be a result of the slight variability of the structures or dynamics in solution that cannot be revealed at the resolution of this study.

Although the L127Δ Fe protein is essentially inactive, it is competent in MgATP and MgADP binding; therefore, we have conducted a parallel study examining the effects on SAXS curves in the presence of saturating concentrations of MgADP and MgATP (Figure 4B). The differences in the scattering curves of the L127Δ Fe protein in comparing the nucleotide-free and nucleotide-bound forms are more pronounced than those observed for the native Fe protein. In addition, the R_g values of the L127Δ Fe protein are decreased by ∼1 Å upon addition of nucleotides to more closely approximate the R_g values of the nucleotide-free Fe protein obtained by simulation. This suggests that the L127Δ Fe protein, in the presence of MgADP or MgATP, undergoes a conformational change that is likely manifested in movement of the subunits toward a more globular structure or toward a conformation that more closely approximates the structure observed crystallographically for the L127Δ Fe protein. The variance in the observed R_g values may reflect a larger degree of conformational flexibility in the L127Δ Fe protein dimer in comparison to the native Fe protein. This is likely to be

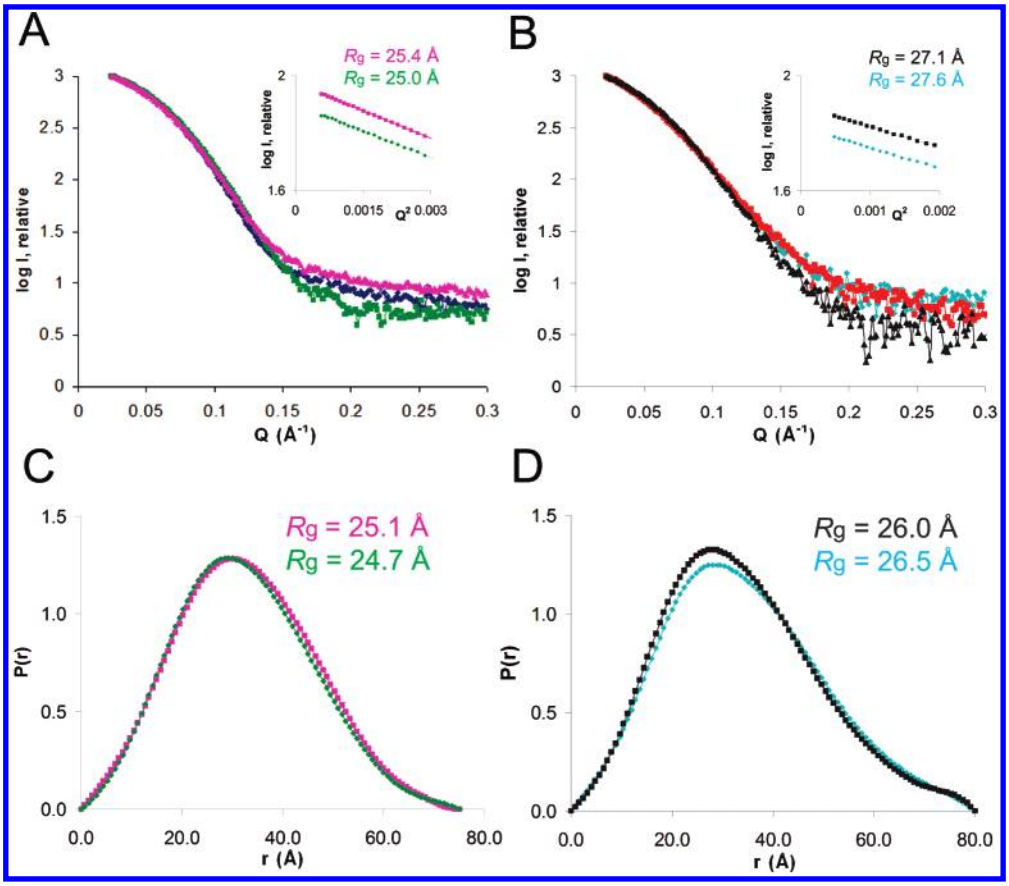

FIGURE 4: (A) Experimental scattering curves of nucleotide-free Fe protein (blue) along with nucleotide-bound conformations of 5 mg/mL native Fe protein incubated with 5 mM MgATP (magenta) or MgADP (green) and Guinier plots for Fe protein with bound MgATP (magenta) and MgADP (green) as inset A. (B) Experimental scattering curves of nucleotide-free L127Δ Fe protein (red), along with nucleotide-bound conformations of 5 mg/mL L127Δ Fe protein incubated with 5 mM MgATP (gray) or MgADP (aqua) and Guinier plots for Fe protein with bound MgATP (gray) and MgADP (aqua) as inset A. (C and D) Pair distribution function plots generated from scattering curves A and B, respectively, with calculated R_g values for the native Fe protein with MgATP (magenta) and MgADP (green) and calculated R_g values for the L127Δ Fe protein with MgATP (gray) and MgADP (aqua).

a result of the relatively small number of intersubunit interactions in the L127Δ Fe protein. Recently, the structure of the L127Δ Fe protein with bound MgATP was determined (*34*). This structure was generated by soaking crystals of the nucleotide-free state of the L127 Å Fe protein with MgATP just prior to cryo-cooling for data collection. The crystal structure of the MgATP-bound state did not differ in overall conformation or the relationship between the two subunits of the dimer when compared to the nucleotide-free form of the L127Δ Fe protein. The observation that these two structures have the same overall shape crystallographically but clearly differing shapes in solution strongly suggests that the limited intersubunit contacts allow for a more flexible structure in solution, and multiple states distinct from the native Fe protein structure can be observed; thus, the crystalline lattice in this case may be stabilizing a local minimum energy structure. The apparent conformational flexibility of the L127Δ Fe protein not withstanding, the overall conclusion of this work is clearly that the more elongated structure of the L127Δ Fe protein observed by crystallography predominates in solution, and the idea that this state is not a faithful mimic of the MgATP state is well supported.

SUMMARY AND CONCLUSIONS

In this study, SAXS was used to probe and analyze the structure of the nitrogenase Fe protein in defined states in solution. The results described herein established that the more elongated L127Δ Fe protein conformation observed in the crystal structure predominates in solution. Using the crystal structures of the native Fe protein, the MgADP-bound state of the native Fe protein, and the L127Δ Fe protein as benchmarks, it is concluded that the structure of the L127Δ Fe protein observed crystallographically either in the presence or in the absence of bound nucleotides does not closely resemble the MgATP-bound conformation of the Fe protein in solution.

The proposal that the L127Δ Fe protein might mimic the conformation of the MgATP-bound state of the Fe protein was based on the results of a wealth of biochemical and spectroscopic experiments that indicate clear parallels between the biochemical and spectroscopic properties of the L127Δ Fe protein and the native Fe protein in the presence of bound MgATP. In addition, it was shown that the L127Δ Fe protein was capable of undergoing a conformational change in the presence of the MoFe protein to form a stable complex that closely resembles the Fe protein−MoFe protein complex stabilized in the presence of MgADP and tetrafluo-

roaluminate (*37*). Since the overall solution structures of the L127Δ Fe protein and the MgATP-bound state of the Fe protein, as determined by SAXS, do not appear to closely resemble each other, these results suggest that similar complexes can therefore be formed via at least two different pathways of Fe protein conformational change triggered by the MoFe protein. Also, apparently similar spectroscopic and biochemical properties, including similarities in EPR spectral features and metal chelation properties, can be obtained by markedly different protein conformations. This indicates the need to further dissect the factors that influence the spectroscopic and electronic structure properties of the [4Fe-4S] cluster of the Fe protein.

REFERENCES

1. Peters, J. W., and Szilagyi, R. K. (2006) Exploring new frontiers of nitrogenase structure and mechanism, *Curr. Opin. Chem. Biol. 10*, 101−108.
2. Howard, J. B., and Rees, D. C. (2006) How many metals does it take to fix N_2? A mechanistic overview of biological nitrogen fixation, *Proc. Natl. Acad. Sci. U.S.A. 103*, 17088−17093.
3. Barney, B. M., Lee, H. I., Dos Santos, P. C., Hoffman, B. M., Dean, D. R., and Seefeldt, L. C. (2006) Breaking the N_2 triple bond: Insights into the nitrogenase mechanism, *Dalton Trans.*, 2277−2284.
4. Dos Santos, P. C., Igarashi, R. Y., Lee, H. I., Hoffman, B. M., Seefeldt, L. C., and Dean, D. R. (2005) Substrate interactions with the nitrogenase active site, *Acc. Chem. Res. 38*, 208−214.
5. Sprang, S. R. (1997) G protein mechanisms: Insights from structural analysis, *Annu. Rev. Biochem. 66*, 639−678.
6. Sunahara, R. K., Tesmer, J. J., Gilman, A. G., and Sprang, S. R. (1997) Crystal structure of the adenylyl cyclase activator $G_{s\alpha}$, *Science 278*, 1943−1947.
7. Sondek, J., Lambright, D. G., Noel, J. P., Hamm, H. E., and Sigler, P. B. (1994) GTPase mechanism of G proteins from the 1.7-Å crystal structure of transducin α-GDP-AlF_4^-, *Nature 372*, 276−279.
8. Kjeldgaard, M., and Nyborg, J. (1992) Refined structure of elongation factor EF-Tu from *Escherichia coli*, *J. Mol. Biol. 223*, 721−742.
9. Jurnak, F. (1985) Structure of the GDP domain of EF-Tu and location of the amino acids homologous to *ras* oncogene proteins, *Science 230*, 32−36.
10. Story, R. M., and Steitz, T. A. (1992) Structure of the recA protein-ADP complex, *Nature 355*, 374−376.
11. Story, R. M., Weber, I. T., and Steitz, T. A. (1992) The structure of the *E. coli* recA protein monomer and polymer, *Nature 355*, 318−325.
12. Rayment, I. (1996) The structural basis of the myosin ATPase activity, *J. Biol. Chem. 271*, 15850−15853.
13. Rayment, I., Holden, H. M., Whittaker, M., Yohn, C. B., Lorenz, M., Holmes, K. C., and Milligan, R. A. (1993) Structure of the actin-myosin complex and its implications for muscle contraction, *Science 261*, 58−65.
14. Rayment, I., Rypniewski, W. R., Schmidt-Base, K., Smith, R., Tomchick, D. R., Benning, M. M., Winkelmann, D. A., Wesenberg, G., and Holden, H. M. (1993) Three-dimensional structure of myosin subfragment-1: A molecular motor, *Science 261*, 50−58.
15. Lowe, D. J., and Thorneley, R. N. (1984) The mechanism of *Klebsiella pneumoniae* nitrogenase action. The determination of rate constants required for the simulation of the kinetics of N_2 reduction and H_2 evolution, *Biochem. J. 224*, 895−901.
16. Thorneley, R. N., and Lowe, D. J. (1984) The mechanism of *Klebsiella pneumoniae* nitrogenase action. Pre-steady-state kinetics of an enzyme-bound intermediate in N_2 reduction and of NH_3 formation, *Biochem. J. 224*, 887−894.
17. Barney, B. M., Laryukhin, M., Igarashi, R. Y., Lee, H. I., Dos Santos, P. C., Yang, T. C., Hoffman, B. M., Dean, D. R., and Seefeldt, L. C. (2005) Trapping a hydrazine reduction intermediate on the nitrogenase active site, *Biochemistry 44*, 8030−8037.
18. Ryle, M. J., Lanzilotta, W. N., and Seefeldt, L. C. (1996) Elucidating the mechanism of nucleotide-dependent changes in the redox potential of the [4Fe-4S] cluster in nitrogenase iron protein: The role of phenylalanine 135, *Biochemistry 35*, 9424−9434.
19. Lanzilotta, W. N., Holz, R. C., and Seefeldt, L. C. (1995) Proton NMR investigation of the $[4Fe\text{-}4S]^{1+}$ cluster environment of nitrogenase iron protein from *Azotobacter vinelandii*: Defining nucleotide-induced conformational changes, *Biochemistry 34*, 15646−15653.
20. Deits, T. L., and Howard, J. B. (1989) Kinetics of MgATP-dependent iron chelation from the Fe-protein of the *Azotobacter vinelandii* nitrogenase complex. Evidence for two states, *J. Biol. Chem. 264*, 6619−6628.
21. Howard, J. B., and Rees, D. C. (1994) Nitrogenase: A nucleotide-dependent molecular switch, *Annu. Rev. Biochem. 63*, 235−264.
22. Lindahl, P. A., Day, E. P., Kent, T. A., Orme-Johnson, W. H., and Munck, E. (1985) Mossbauer, EPR, and magnetization studies of the *Azotobacter vinelandii* Fe protein. Evidence for a $[4Fe\text{-}4S]^{1+}$ cluster with spin S = 3/2, *J. Biol. Chem. 260*, 11160−11173.
23. Lindahl, P. A., Gorelick, N. J., Munck, E., and Orme-Johnson, W. H. (1987) EPR and Mossbauer studies of nucleotide-bound nitrogenase iron protein from *Azotobacter vinelandii*, *J. Biol. Chem. 262*, 14945−14953.
24. Ljones, T., and Burris, R. H. (1978) Nitrogenase: The reaction between the Fe protein and bathophenanthrolinedisulfonate as a probe for interactions with MgATP, *Biochemistry 17*, 1866−1872.
25. Lanzilotta, W. N., Fisher, K., and Seefeldt, L. C. (1997) Evidence for electron transfer-dependent formation of a nitrogenase iron protein-molybdenum-iron protein tight complex. The role of aspartate 39, *J. Biol. Chem. 272*, 4157−4165.
26. Walker, G. A., and Mortenson, L. E. (1974) Effect of magnesium adenosine 5′-triphosphate on the accessibility of the iron of clostridial azoferredoxin, a component of nitrogenase, *Biochemistry 13*, 2382−2388.
27. Zumft, W. G., Mortenson, L. E., and Palmer, G. (1974) Electron-paramagnetic-resonance studies on nitrogenase. Investigation of the oxidation-reduction behavior of azoferredoxin and molybdoferredoxin with potentiometric and rapid-freeze techniques, *Eur. J. Biochem. 46*, 525−535.
28. Georgiadis, M. M., Komiya, H., Chakrabarti, P., Woo, D., Kornuc, J. J., and Rees, D. C. (1992) Crystallographic structure of the nitrogenase iron protein from *Azotobacter vinelandii*, *Science 257*, 1653−1659.
29. Schindelin, H., Kisker, C., Schlessman, J. L., Howard, J. B., and Rees, D. C. (1997) Structure of ADP·AlF_4^--stabilized nitrogenase complex and its implications for signal transduction, *Nature 387*, 370−376.
30. Schlessman, J. L., Woo, D., Joshua-Tor, L., Howard, J. B., and Rees, D. C. (1998) Conformational variability in structures of the nitrogenase iron proteins from *Azotobacter vinelandii* and *Clostridium pasteurianum*, *J. Mol. Biol. 280*, 669−685.
31. Jang, S. B., Seefeldt, L. C., and Peters, J. W. (2000) Insights into nucleotide signal transduction in nitrogenase: Structure of an iron protein with MgADP bound, *Biochemistry 39*, 14745−14752.
32. Tezcan, F. A., Kaiser, J. T., Mustafi, D., Walton, M. Y., Howard, J. B., and Rees, D. C. (2005) Nitrogenase complexes: Multiple docking sites for a nucleotide switch protein, *Science 309*, 1377−1380.
33. Sen, S., Igarashi, R., Smith, A., Johnson, M. K., Seefeldt, L. C., and Peters, J. W. (2004) A conformational mimic of the MgATP-bound "on state" of the nitrogenase iron protein, *Biochemistry 43*, 1787−1797.
34. Sen, S., Krishnakumar, A., McClead, J., Johnson, M. K., Seefeldt, L. C., Szilagyi, R. K., and Peters, J. W. (2006) Insights into the role of nucleotide-dependent conformational change in nitrogenase catalysis: Structural characterization of the nitrogenase Fe protein Leu127 deletion variant with bound MgATP, *J. Inorg. Biochem. 100*, 1041−1052.
35. Schmid, B., Einsle, O., Chiu, H. J., Willing, A., Yoshida, M., Howard, J. B., and Rees, D. C. (2002) Biochemical and structural characterization of the cross-linked complex of nitrogenase: Comparison to the ADP-AlF4$^-$-stabilized structure, *Biochemistry 41*, 15557−15565.
36. Ryle, M. J., and Seefeldt, L. C. (1996) Elucidation of a MgATP signal transduction pathway in the nitrogenase iron protein: Formation of a conformation resembling the MgATP-bound state by protein engineering, *Biochemistry 35*, 4766−4775.
37. Chiu, H., Peters, J. W., Lanzilotta, W. N., Ryle, M. J., Seefeldt, L. C., Howard, J. B., and Rees, D. C. (2001) MgATP-bound and

nucleotide-free structures of a nitrogenase protein complex between the Leu 127Δ-Fe-protein and the MoFe-protein, *Biochemistry 40*, 641−650.

38. Lanzilotta, W. N., Fisher, K., and Seefeldt, L. C. (1996) Evidence for electron transfer from the nitrogenase iron protein to the molybdenum-iron protein without MgATP hydrolysis: Characterization of a tight protein-protein complex, *Biochemistry 35*, 7188−7196.
39. Smolsky, I. L., Liu, P., Niebuhr, M., Ito, L., Weiss, T. M., and Tsuruta, H. (2007) Biological small-angle X-ray scattering facility at the Stanford Synchrotron Radiation Laboratory, *J. Appl. Crystallogr. 40*, s453−s458.
40. Krigbaum, W. R., and Kügler, F. R. (1970) Molecular conformation of egg-white lysozyme and bovine α-lactalbumin in solution, *Biochemistry 9*, 1216−1223.
41. Vaney, M. C., Maignan, S., Ries-Kautt, M., and Ducriux, A. (1996) High-resolution structure (1.33 Å) of a HEW lysozyme tetragonal crystal grown in the APCF apparatus. Data and structural comparison with a crystal grown under microgravity from SpaceHab-01 mission, *Acta Crystallogr. D52*, 505−517.
42. Svergun, D., Barberato, C., and Koch, M. (1995) CRYSOL: A program to evaluate X-ray solution scattering of biological macromolecules from atomic coordinates, *J. Appl. Crystallogr. 28*, 768−773.
43. Svergun, D. (1992) Determination of the regularization parameter in indirect-transform methods using perceptual criteria, *J. Appl. Crystallogr. 25*, 495−503.
44. Svergun, D. I. (1999) Restoring low resolution structure of biological macromolecules from solution scattering using simulated annealing, *Biophys. J. 76*, 2879−2886.
45. Kozin, M. B., and Svergun, D. I. (2001) Automated matching of high- and low-resolution structural models, *J. Appl. Crystallogr. 34*, 33−41.
46. Volkov, V. V., and Svergun, D. I. (2003) Uniqueness of ab initio shape determination in small-angle scattering, *J. Appl. Crystallogr. 36*, 860−864.
47. Chen, L., Gavini, N., Tsuruta, H., Eliezer, D., Burgess, B. K., Doniach, S., and Hodgson, K. O. (1994) MgATP-induced conformational changes in the iron protein from *Azotobacter vinelandii*, as studied by small-angle X-ray scattering, *J. Biol. Chem. 269*, 3290−3294.
48. Grossmann, G. J., Hasnain, S. S., Yousafzai, F. K., and Eady, R. R. (2001) Evidence for the selective population of FeMo cofactor sites in MoFe protein and its molecular recognition by the Fe Protein in transition state complex analogues of nitrogenase, *J. Biol. Chem. 276*, 6582−6590.

BI700446S